Third generation of the Potsdam Magnetic Model of the Earth (POMME)

S. Maus

CIRES, University of Colorado, Boulder, Colorado 80302, USA

National Geophysical Data Center, NOAA E/GC1, 325 Broadway, Boulder, Colorado 80305-3328, USA (stefan.maus@noaa.gov)

M. Rother, C. Stolle, W. Mai, S. Choi, and H. Lühr

GeoForschungsZentrum, Telegrafenberg, D-14473 Potsdam, Germany (rother@gfz-potsdam.de)

D. Cooke

Air Force Research Laboratory, 29 Randolph Road, Hanscom Air Force Base, Massachusetts 01731, USA

C. Roth

AER/Radex Inc., Lexington, Massachusetts 02421, USA

[1] The Potsdam Magnetic Model of the Earth (POMME) is a geomagnetic field model providing an estimate of the Earth's core, crustal, magnetospheric, and induced magnetic fields. The internal field is represented to spherical harmonic (SH) degree 90, while the secular variation and acceleration are given to SH degree 16. Static and time-varying magnetospheric fields are parameterized in Geocentric Solar-Magnetospheric (GSM) and Solar-Magnetic (SM) coordinates and include Disturbance Storm-Time (Dst index) and Interplanetary Magnetic Field (IMF-By) dependent contributions. The model was estimated from five years of CHAMP satellite magnetic data. All measurements were corrected for ocean tidal induction and night-side ionospheric F-region currents. The model is validated using an independent model from a combined data set of Ørsted and SAC-C satellite measurements. For the core field to SH degree 13, the root mean square (RMS) vector difference between the two models at the center of the model period is smaller than 4 nT at the Earth's surface. The RMS uncertainty increases to about 100 nT for the predicted field in 2010, as inferred from the difference between the two models.

1. Introduction

[2] The recent satellite magnetic missions Ørsted, CHAMP and SAC-C have provided the data basis for a new generation of highly accurate main field models [*Olsen et al.*, 2000, 2006; *Olsen*, 2002; *Holme et al.*, 2002; *Maus et al.*, 2005a; *Lesur et al.*, 2005]. Typically, these models include the following:

[3] 1. A static internal field including core and crustal fields.

[4] 2. The secular variation.

[5] 3. The secular acceleration.

[6] 4. A time-averaged magnetospheric field, including induction infects due to Earth rotation [*Maus and Lühr*, 2005].

[7] 5. A time-varying magnetospheric field, coupled to the Est/Ist index [*Maus and Weidelt*, 2004; *Olsen et al.*, 2005] and to the Y-component of the interplanetary magnetic field [*Lesur et al.*, 2005].

[8] In particular, seven years of continuous measurements have made it possible to determine the temporal derivatives of the core field with unprecedented accuracy.

[9] Here, we describe the third generation of the Potsdam Magnetic Model of the Earth (POMME), which is a geomagnetic field model providing an estimate of the Earth's core, crustal, magnetospheric and induced magnetic fields. The first generation, POMME-1.4 [*Maus et al.*, 2005a], released in May 2003, was the parent model for the candidate models of GeoForschungsZentrum Potsdam for the 9th generation International Geomagnetic Reference Field (IGRF). POMME-1.4 was estimated from Ørsted and CHAMP vector data up to July 2002. It had a parameterization of the internal field to spherical harmonic (SH) degree 15, secular variation to degree 15, and acceleration to degree 10. It included axi-symmetric external and induced fields in Solar-Magnetic (SM) coordinates tracked by the Dst index, and a stable degree-2 external field in Geocentric Solar-Magnetospheric (GSM) coordinates. Corrections for the CHAMP star camera misalignment were coestimated as part of the model.

[10] In a major revision, the second generation model POMME-2.5 was based on scalar and vector data from Ørsted, and CHAMP up to July 2004. Because there was a general demand for calibrated CHAMP vector data, and we had developed a stable calibration procedure, the CHAMP data were now calibrated for the star camera misalignment prior to estimating the model. The ring-current parameterization by Dst was substituted with an improved parameterization using the Est/Ist index [*Maus and Weidelt*, 2004]. An asymmetric ring current in SM coordinates and a contribution in GSM tracked by the Interplanetary Magnetic Field were introduced. The new parameterization included fields induced by stable external fields in a rotating Earth [*Maus and Lühr*, 2005]. The internal field was estimated to degree 60 (POMME-2.4), and was merged with the lithospheric field model MF3 to extend to degree 90 (POMME-2.5). The secular variation and acceleration were given to degrees 18 and 12, respectively. The models POMME 2.2 to 2.4 served as parent models for the NGDC/GFZ candidate models for the 10th generation of IGRF [*Maus et al.*, 2005b] and the World Magnetic Model 2005 [*McLean et al.*, 2004].

[11] As described in the following, the third generation of POMME makes use of the latest satellite magnetic data, largely retaining the parameterization of the previous generation. Due to the limited quality and availability of Ørsted vector data, it was decided to base the model entirely on CHAMP data, using an independent Ørsted/SAC-C model only for model validation.

2. Input Data

[12] There are presently three satellites with science quality magnetometers in low-Earth orbit: Ørsted, SAC-C and CHAMP. Ørsted scalar data is available with more than 80% coverage from 1999 to present, while Ørsted vector data has a coverage of about 45% and is only sporadically available since 2003. The vector magnetometer measurements on SAC-C could never be utilized due to the malfunction of the star camera, but its scalar magnetometer provided a data coverage of more than 70% from 2001 to the end of 2004. For CHAMP, scalar and vector data are almost continuously available since the start of the mission in mid 2000. The data used in this study are summarized in Table 1. Ørsted and SAC-C data were only used for an independent control model. Due to their large polar gap, lower quality and incomplete temporal coverage, these

Table 1. Summary of Vector and Scalar Measurements Used in This Study[a]

	S. Polar	Midlatitude	N. Polar	Day Range	Raw Data Coverage
CHAMP Vector		637,622		207 to 2069	94.5%
CHAMP Scalar	217,128	1,061,386	195,416	207 to 2068	99.2%
Ørsted Vector		423,511		−291 to 1651	44.4%
Ørsted Scalar	251,938	1,612,318	205,265	−291 to 2069	82.9%
SAC-C Scalar	156,063	850,472	138,602	388 to 1742	71.7%

[a] S. polar tracks are below −50°, N. polar tracks are above 50°, and midlatitude tracks cover the overlapping range of −60° to 60° magnetic latitude. Also given are the day number intervals for which data were available. Day number zero is 1-Jan-2000, 00:00 UT. The right column notes the coverage of the raw data set during this period.

data are less qualified for field modeling. The final POMME-3 model is therefore based entirely on CHAMP data.

3. Data Selection

[13] We follow the data selection procedures which are generally used in main field modeling. For CHAMP data, we discard all tracks which were identified as being contaminated by magnetic signals due to plasma instabilities in the ionospheric F-region [*Stolle et al.*, 2006]. To reduce attitude uncertainty, CHAMP vector data are only used when the star camera is in dual-head mode. The data selection criteria are summarized in Table 2. Different criteria are applied to midlatitude and high-latitude data in order to account for the difference in the properties of data collected in these regions. The primary differences are (1) the higher noise level of high latitude data due to auroral current systems, which is partly compensated by (2) the much denser spatial data coverage due to the geometry of the satellite orbits. For the POMME model, high-latitude tracks were defined as covering the regions poleward of |50°|, and midlatitude tracks covering the overlapping range of −60° to 60°, magnetic latitude.

[14] Finally, the residuals against POMME-2.5 on all tracks and in all data sets were plotted in terms of RMS against longitude, and RMS against time, in order to identify and discard remaining tracks with abnormally high noise level.

4. Data Processing

[15] Several corrections were applied to the data, namely for the misalignment of the CHAMP star camera, for ambient plasma effects, and for ocean tidal induction.

4.1. Correction for CHAMP Star Camera Misalignment

[16] Every satellite vector magnetometer requires an in-flight calibration of the angles between the coordinate systems of the star camera and the vector magnetometer. For CHAMP, final level-3 data are not yet available and the level-2 data require the user to apply a star camera misalignment correction. As a preliminary calibration, we have estimated a continuous time series of the misalignment angles. A 3-day window was moved over the CHAMP vector data set. From the night-side data in the range of −60° to +60° magnetic latitude, three misalignment correction angles were estimated by minimizing the root mean square (RMS) of the vector component residuals, after subtracting the field model POMME-2.5. Once the time series of misalignment angles has been estimated, a simple point-by-point correction can be applied to all CHAMP vector data. The calibration file, a C-language procedure callable from FORTRAN, and a Matlab interface are available at http://www.gfz-potsdam.de/pb2/pb23/SatMag/sca.html.

4.2. Correction for Ocean Tidal Magnetic Fields

[17] The ocean dynamo contributes up to about 3 nT to the magnetic field measured at satellite

Table 2. Summary of Data Selection Criteria[a]

	Midlatitude	High Latitude
Kp $\leq$ 2	√	√
3 hours earlier: Kp $\leq$ 2	√	√
$|Dst| \leq 30$	√	√
$|\partial_t Dst| \leq 2$ nT/h	√	√
$E_m \leq 0.8$ mV/m		√
$21{:}00 \leq LT \leq 5{:}00$	√	
CHAMP: dual-head SC mode	√	√
CHAMP: no plasma irregularities	√	

[a] Here, Kp and Dst are magnetic indices, E_m is the merging electric field at the magnetopause, and SC stands for star camera.

altitude. This is a rather small effect. However, since it can be accurately predicted [*Kuvshinov and Olsen*, 2005], one may as well subtract this effect. We use the predictions of Kuvshinov, which are available at http://www.gfz-potsdam.de/pb2/pb23/SatMag/ocean_tides.html.

4.3. Correction for Diamagnetic Effect

[18] Plasma pressure-driven electric currents reduce the magnetic field in the ionospheric F-region by a few nanotesla. This effect is particularly important for CHAMP, with its orbital altitude close to the peak ionospheric plasma density. CHAMP has a Langmuir Probe which measures the ambient electron density and temperature. Using these Langmuir Probe measurements, the magnetic field readings of CHAMP were corrected using the approximate formula for the diamagnetic effect given by *Lühr et al.* [2003]. For Ørsted and SAC-C, similar corrections could be applied using an ionospheric model. However, since the effect is much smaller at their higher altitude, such a correction was not applied here.

4.4. Correction for Gravity-Driven Ionospheric Currents

[19] The gravity-driven current system in the ionospheric F-region generates a significant magnetic signal of the order of 5 nT *Maus and Lühr* [2006]. In contrast to the approximation used for the pressure-driven current, its magnetic signal is equally strong outside of the ionosphere. We therefore corrected the data of all three satellites for this effect. We used the ion densities from the International Reference Ionosphere, IRI-2000 [*Bilitza*, 2001], and determined the primary gravity-driven current on 46 horizontal shells with a vertical spacing of 20 km. For each shell, we then found the nondivergent, freely flowing part of the current. Integrating over the magnetic effects of the currents in all shells, we obtained the magnetic signal at the measurement locations along the satellite orbit. Further details of the correction are given by *Maus and Lühr* [2006].

5. Model Parameterization and Estimation

[20] For the external magnetic field we used the model of *Maus and Lühr* [2005]. Such an external field model cannot be coestimated from night-side-only data. We verified the published coefficient values on a new 24h data set of CHAMP and

Ørsted data, finding such small differences that it was not justified to introduce an updated set of coefficients. Therefore the new POMME model uses the values of the coefficients given by *Maus and Lühr* [2005] for the magnetospheric part of the geomagnetic field. This includes the separation of the Dst effect into the Est and Ist parts [*Maus and Weidelt*, 2004].

[21] Following *Lesur et al.* [2005] and *Olsen et al.* [2006], we coestimate a residual time-varying axial degree-1 external field in SM coordinates since the Dst index is known to have occasional baseline problems. A bin width of one day was chosen in order to prevent the aliasing of spatial effects, since a satellite covers the Earth with 15 orbits during 24h. Of course, fields with a SH order larger than the Nyquest frequency for 15 samples ($m > 7$) could still alias into this external field estimate. Coestimating a daily offset to the degree-1 external field is intended to correct for Dst baseline uncertainties. Indeed, this has been found to improve the estimated temporal derivatives of the internal field [*Lesur et al.*, 2005; *Olsen et al.*, 2006].

[22] The internal field is parameterized in the usual way as

$$V(r,\vartheta,\varphi,t) = R \sum_{\ell=1}^{N} \left(\frac{R}{r}\right)^{\ell+1} \sum_{m=-\ell}^{\ell} g_\ell^m \breve{\beta}_\ell^m(\vartheta,\varphi), \quad (1)$$

where r, ϑ and φ are the radius, colatitude and longitude, respectively, $R = 6371.2$ km is the traditional geomagnetic reference radius, N is the degree of the expansion, g_ℓ^m are the SH coefficients of the lithospheric field, and $\breve{\beta}_\ell^m(\vartheta, \varphi)$ are Schmidt seminormalized surface spherical harmonic functions in the convenient notation of *Backus et al.* [1996, p. 141]

$$\breve{\beta}_\ell^m = \cos m\phi \breve{P}_\ell^m(\cos \theta), \quad 0 \le m \le \ell \quad (2)$$

$$\breve{\beta}_\ell^{-m} = \sin m\phi \breve{P}_\ell^m(\cos \theta), \quad 1 \le m \le \ell. \quad (3)$$

Here, the functions $\breve{P}_\ell^m(\mu)$ are defined as

$$\breve{P}_\ell^m(\mu) = \begin{cases} \sqrt{2\frac{(\ell-m)!}{(\ell+m)!}} P_\ell^m(\mu) & \text{if } 1 \le m \le \ell \\ P_\ell(\mu) & \text{if } m = 0, \end{cases} \quad (4)$$

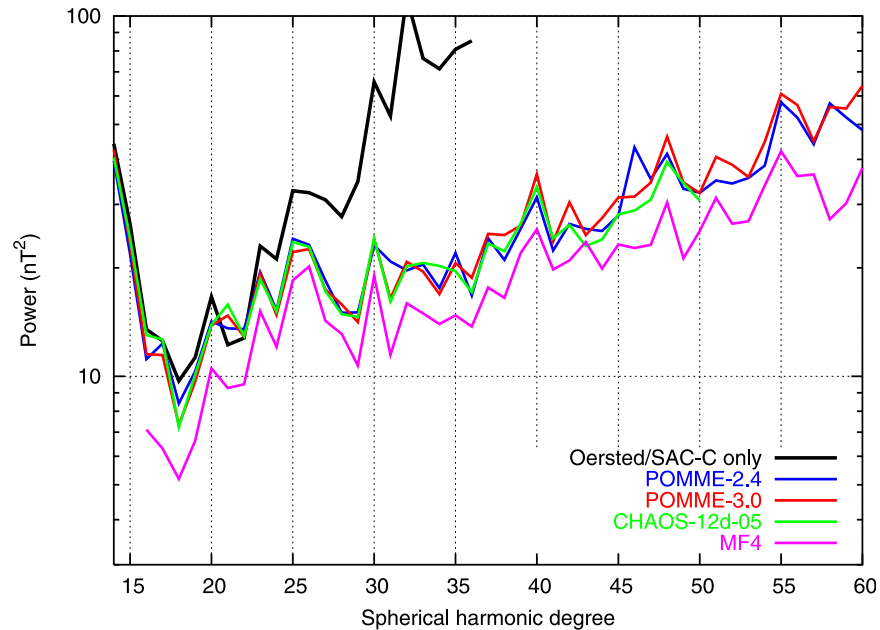where $P_\ell^m(\mu)$ are the associated Legendre functions [*Backus et al.*, 1996, equation 3.7.2].

Figure 1. Power spectra of the static part of the internal field at the Earth's surface for our independent models from CHAMP (POMME-3.0) and from Ørsted/SAC-C data in comparison with the previous POMME-2.4 model, the CHAOS model [*Olsen et al.*, 2006], and the dedicated lithospheric field model MF4 [*Maus et al.*, 2006].

[23] Accounting for the time change of the core field, each Gauss coefficient is given as a truncated Taylor expansion

$$g(t) = g + tg' + 0.5t^2 g''. \qquad (5)$$

The coefficients g were estimated to SH degree 60, while the secular variation g' and acceleration g'' were estimated to degree 16.

[24] We used a direct solver for the least squares problem, via eigenvectors and eigenvalues of the normal equations. No regularization was applied to the Gauss coefficients of the static part of the field. For the secular variation, degrees 14–16 were damped to impose a decreasing spectrum of g', and degrees 10–16 of g'' were damped to impose a decreasing spectrum of g''. The optimum damping was found by trial and error. It was imposed by adding an appropriate function of the degree ℓ and order m to the corresponding diagonal elements in the normal equations matrix.

6. Result and Discussion of Accuracy

[25] We estimate two models from (almost) independent data sets. One is from CHAMP data only, and the other is from the combined Ørsted and SAC-C data. To fill in the large polar gap of Ørsted and SAC-C we added some polar CHAMP data to their data set. This was done in order to avoid having to damp the static coefficients above SH degree 15 of the Ørsted/SAC-C model. We also estimated a combined CHAMP/Ørsted/SAC-C model. However, this did not lead to an obvious improvement (as can be inferred from the noise level in the secular variation and acceleration) and we therefore decided to declare the CHAMP-only model as the new POMME.

[26] The power spectrum of the static part of the internal field is displayed in Figure 1. Shown are the CHAMP-only model (POMME-3.0), the combined Ørsted/SAC-C model, and two models which are not part of this study, but are shown for comparison. One is the CHAOS model [*Olsen et al.*, 2006], and the other is the dedicated lithospheric field model MF4 [*Maus et al.*, 2006]. The spectra indicate a higher noise level of our Ørsted/SAC-C model, which is partly due to the higher orbital altitude of these two satellites. Furthermore, the spectra show a significantly lower power of MF4. This is due to the along-track filtering of the data used for MF4. The filter is designed to remove spurious long-wavelength external and induced fields which are the dominant source of noise in the input data. Unfortunately, this filter also removes some genuine lithospheric field. As can be seen from the spectra, the effect of contaminating external fields increases with increasing SH degree. Toward higher SH degrees a model from
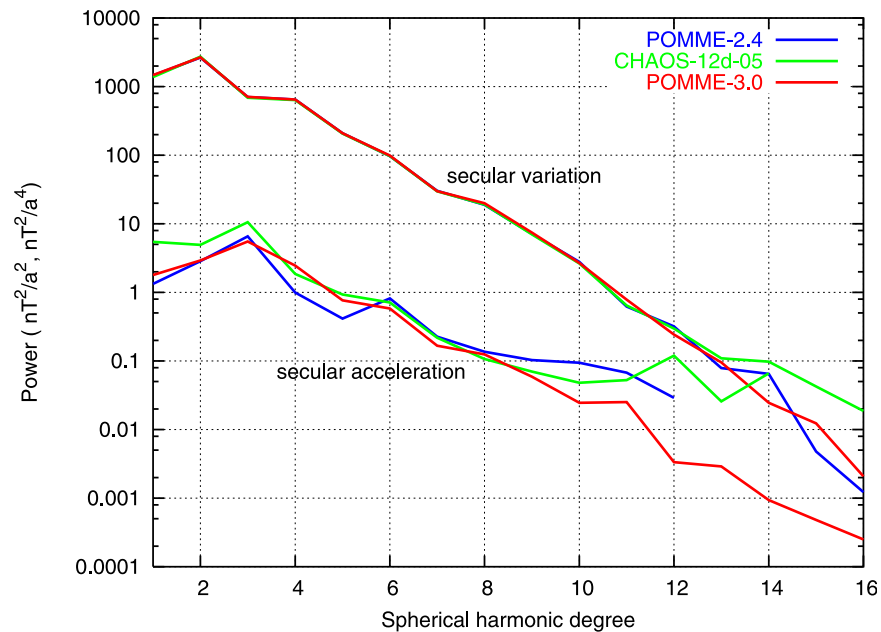
Figure 2. Power spectra of the first and second time derivative of the internal field at the Earth's surface for the new POMME-3.0 model from CHAMP data, in comparison with the previous POMME-2.4 and the CHAOS model by *Olsen et al.* [2006] for 2002.5. The time derivatives of these three models are partly damped.

filtered data, such as MF4, is therefore preferable over a model from unfiltered data.

[27] Figure 2 shows the power spectra of the secular variation and secular acceleration. Due to the different damping used, these spectra do not directly provide information on the relative accuracy of the models.

[28] Finally, the inversion included the coestimation of a residual time-varying, axial, degree-1 external field (q_1^0) in magnetic coordinates. These
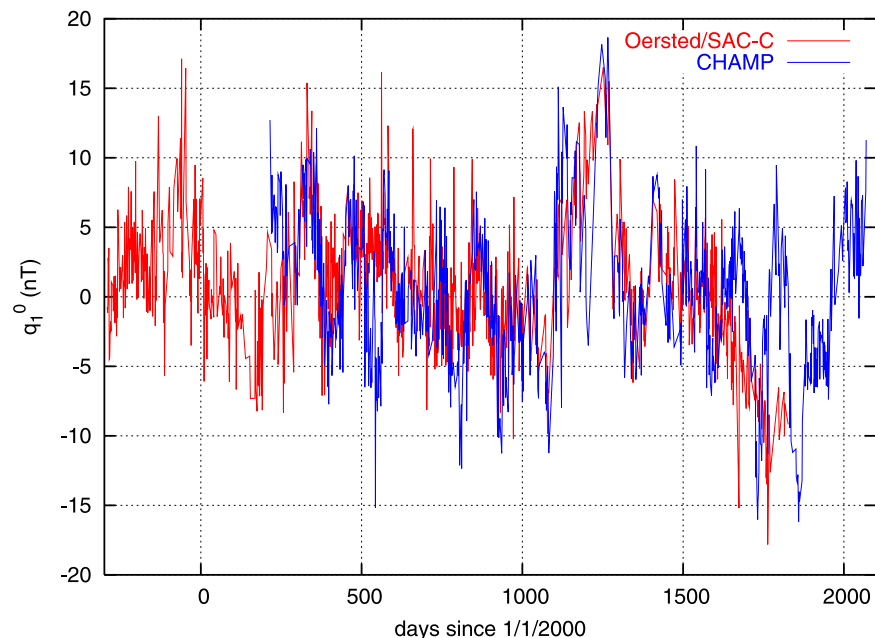

Figure 3. Time series of the daily offsets in the external, uniform field (q_1^0), aligned with the magnetic dipole. The estimates from CHAMP and from Ørsted/SAC-C data agree rather well. Differences are mostly due to the asymmetry of the external field, sampled by the satellites in different local time orbits.
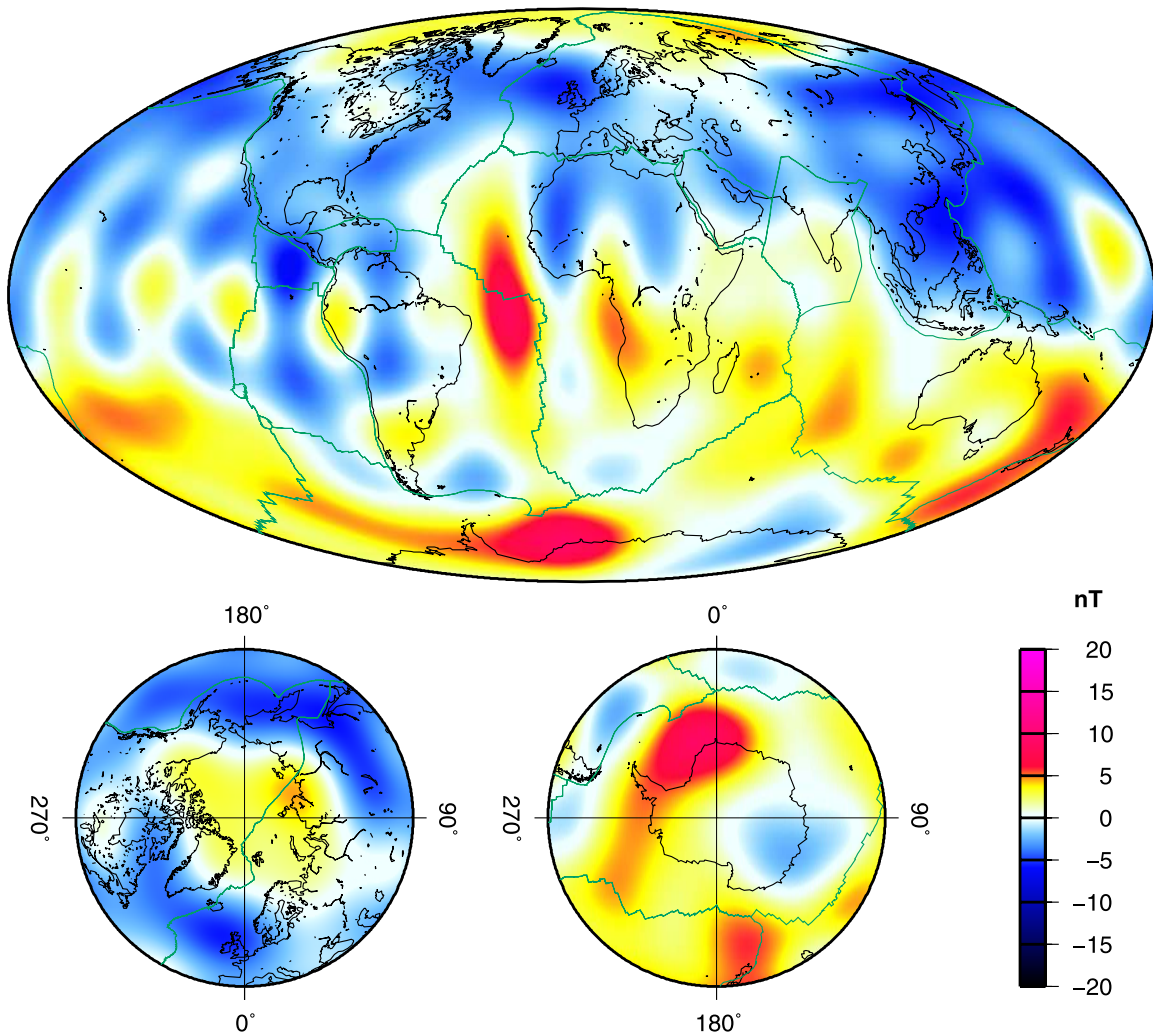
Figure 4. Map of the difference between our independent models from CHAMP and from Ørsted/SAC-C data, the former minus the latter. Displayed is the difference in the z-component (positive downward) at the Earth's surface in 2002.0.

fields can be interpreted as baseline error of the Dst index. The time series of q_1^0 for the two models is given in Figure 3. The magnitude of the result is realistic, and the agreement between the two models supports the reliability. Oscillations of the CHAMP estimates with periods of 130 days, partly in disagreement with the results of the other satellites, reflect the local time dependence of the residuals. It takes CHAMP 130 days to sample all local times. The amplitude of the oscillations can be regarded as a measure of the asymmetry of the ring current. In contrast to the CHAOS model, we did not coestimate q_1^1 and q_1^{-1} because our external field already includes time-varying q_1^1 and q_1^{-1} fields correlated with the IMF-By.

[29] For an estimate of model uncertainty, we directly compare our CHAMP and Ørsted/SAC-C models for the internal field to SH degree 13 at the Earth's surface. Figure 4 shows a map of the difference in the vertical component in 2002. The residuals (CHAMP minus Ørsted/SAC-C) are predominantly negative in the northern hemisphere and positive in the south. This means that the CHAMP-based magnetic field model is somewhat weaker. In particular, its dipole moment is 1.3 nT smaller than the dipole moment of the Ørsted/SAC-C based model. For an estimate of the reliability of the predicted field changes, we apply the secular variation and acceleration up to SH degree 13 to both models and compute the RMS vector difference up to SH degree 13, at the Earth's surface, at epochs from 1995 to 2010, shown in Figure 5. As expected, the models agree best in the period during which data are available from all satellites.
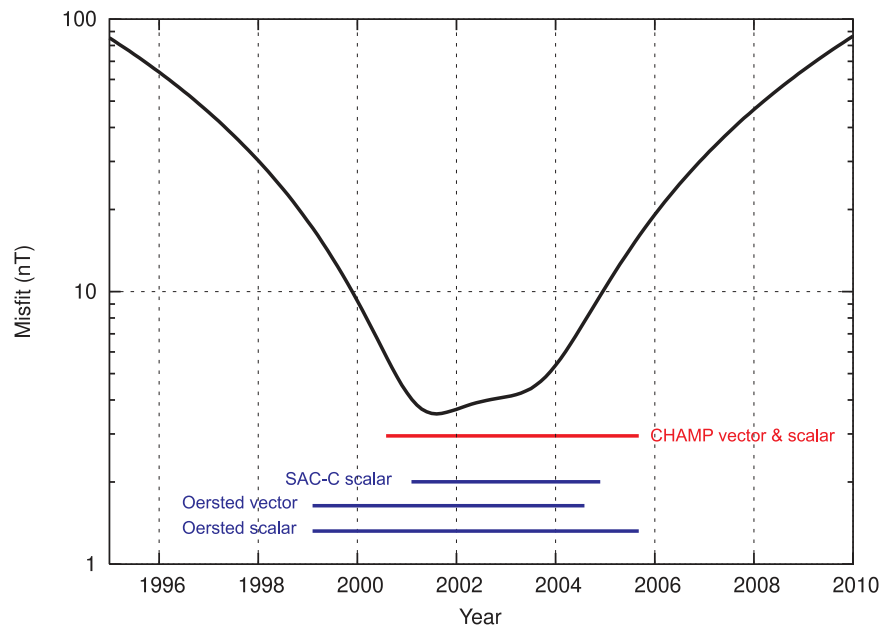
Figure 5. RMS vector difference at the Earth's surface between our independent models from CHAMP and from Ørsted/SAC-C data for the time period from 1995 to 2010. The horizontal bars show the periods for which the respective input data were available. The models were evaluated to SH degree 13, including the secular variation and acceleration to the same SH degree.

The optimum agreement is confined to the time of simultaneous availability of vector data from 2000.5 to 2003.5. The RMS difference between the two models increases to about 100 nT for the predicted core field in 2010. This figure of 100 nT provides an estimate of the uncertainty of the prediction, assuming that the behavior of the core field is entirely determined by its secular variation
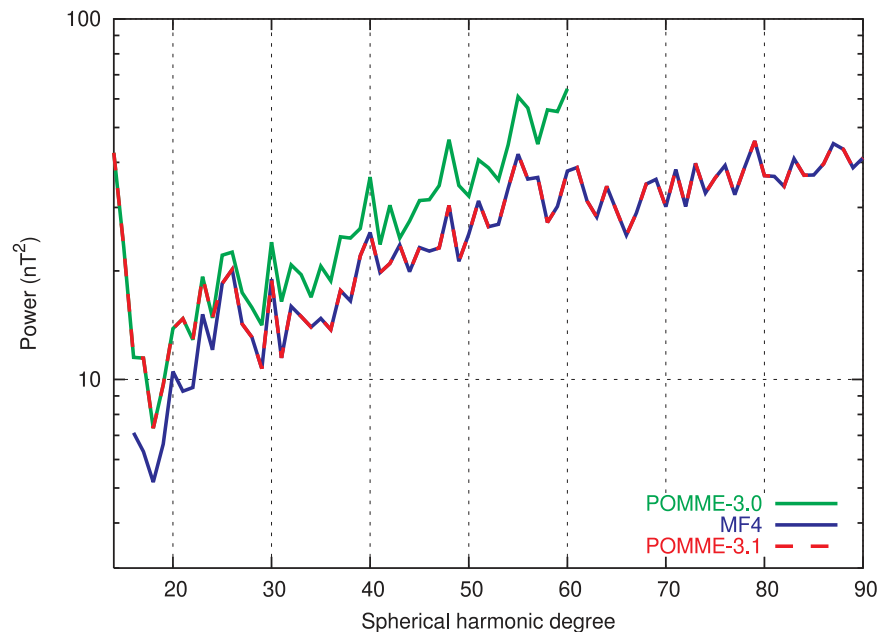

Figure 6. Spectra of the POMME-3.0 and the MF4 models at the Earth's surface. The POMME-3.1 model, overlaid as a dashed line, was constructed by merging the lower-degree portion of POMME-3.0 with the higher-degree portion of MF4. The models were merged at degree 25. At this degree the correlation between the coefficients of the two models reaches a peak value of 0.964.

and acceleration. An additional uncertainty arises from possible changes in the secular acceleration of the field. Such sudden changes in the secular acceleration are visible in historical ground magnetic observatory records and are generally referred to as jerks.

7. Model Availability

[30] The model estimated from CHAMP data is declared as POMME-3.0. For high internal SH degrees, a superior representation of the field is given by the dedicated lithospheric field model MF4 [*Maus et al.*, 2006W], which was also produced only from CHAMP data. We therefore merge degrees 1 to 24 of POMME-3.0 with degrees 25 to 90 of MF4 to produce the final model POMME-3.1. The spectra of these models are shown in Figure 6. The coefficients of POMME-3.0 and POMME-3.1, together with software in the languages C, Matlab and IDL, to evaluate the models, is available from our Web sites http://www.gfz-potsdam.de/pb2/pb23/Sat-Mag/pomme3.html and http://geomag.colorado.edu/pomme3.html. The coefficient tables for POMME-3.0 and POMME-3.1 are also available at http://earthref.org. The Ørsted/SAC-C model, which was derived here solely for the purpose of verifying the accuracy of POMME-3.0, is available from the authors on request.

Acknowledgments

References

Backus, G., R. L. Parker, and C. Constable (1996), *Foundations of Geomagnetism*, Cambridge Univ. Press, New York.

Bilitza, D. (2001), International Reference Ionosphere 2000, *Radio Sci.*, 36, 261–275.

Holme, R., N. Olsen, M. Rother, and H. Lühr (2002), CO2 - A CHAMP magnetic field model, in *CHAMP Mission Results I*, edited by C. Reigber, H. Lühr, and P. Schwintzer, pp. 220–225, Springer, New York.

Kuvshinov, A., and N. Olsen (2005), 3-D modelling of the magnetic field due to ocean tidal flow, in *Earth Observation With CHAMP: Results From Three Years in Orbit*, edited by C. Reigber et al., pp. 359–365, Springer, New York.

Lesur, V., S. Macmillan, and A. Thomson (2005), A magnetic field model with daily variations of the magnetospheric field and its induced counterpart in 2001, *Geophys. J. Int.*, 160, 79–88, doi:10.1111/j.1365-246X.2004.02479.x.

Lühr, H., M. Rother, S. Maus, W. Mai, and D. Cooke (2003), The diamagnetic effect of the equatorial Appleton anomaly: Its characteristics and impact on geomagnetic field modeling, *Geophys. Res. Lett.*, 30(17), 1906, doi:10.1029/2003GL017407.

Maus, S., and H. Lühr (2005), Signature of the quiet-time magnetospheric magnetic field and its electromagnetic induction in the rotating Earth, *Geophys. J. Int.*, 162, 755–763, doi:10.1111/j.1365-246X.2005.02691.x.

Maus, S., and H. Lühr (2006), A gravity-driven electric current in the Earth's ionosphere identified in CHAMP satellite magnetic measurements, *Geophys. Res. Lett.*, 33, L02812, doi:10.1029/2005GL024436.

Maus, S., and P. Weidelt (2004), Separating the magnetospheric disturbance magnetic field into external and transient internal contributions using a 1D conductivity model of the Earth, *Geophys. Res. Lett.*, 31, L12614, doi:10.1029/2004GL020232.

Maus, S., H. Lühr, G. Balasis, M. Rother, and M. Mandea (2005a), Introducing POMME, Potsdam Magnetic Model of the Earth, in *Earth Observation With CHAMP: Results From Three Years in Orbit*, edited by C. Reigber et al., pp. 293–298, Springer, New York.

Maus, S., S. McLean, D. Dater, H. Lühr, M. Rother, W. Mai, and S. Choi (2005b), NGDC/GFZ candidate models for the 10th generation International Geomagnetic Reference Field, *Earth Planets Space*, 57, 1151–1156.

Maus, S., M. Rother, K. Hemant, C. Stolle, H. Lühr, A. Kuvshinov, and N. Olsen (2006), Earth's crustal magnetic field determined to spherical harmonic degree 90 from CHAMP satellite measurements, *Geophys. J. Int.*, 164, 319–330, doi:10.1111/j.1365-246X.2005.02833.x.

McLean, S., S. Macmillan, S. Maus, V. Lesur, A. Thomson, and D. Dater (2004), The US/UK world magnetic model for 2005–2010, NOAA Tech. Rep. NESDIS/NGDC-1, Natl. Oceanic and Atmos. Admin, Silver Spring, Md.

Olsen, N. (2002), A model of the geomagnetic main field and its secular variation for epoch 2000 estimated from Ørsted data, *Geophys. J. Int.*, 149, 454–462.

Olsen, N., et al. (2000), Ørsted initial field model, *Geophys. Res. Lett.*, 27, 3607–3610.

Olsen, N., T. J. Sabaka, and F. Lowes (2005), New parameterization of external and induced fields in geomagnetic field modeling, and a candidate model for IGRF 2005, *Earth Planets Space*, 57(12), 1141–1149.

Olsen, N., H. Lühr, T. J. Sabaka, M. Mandea, M. Rother, L. Tøffner-Clausen, and S. Choi (2006), CHAOS—A model of Earth's magnetic field derived from CHAMP, Ørsted, and SAC-C magnetic satellite data, *Geophys. J. Int.*, doi:10.1111/j.1365-246X.2006.02959.x, in press.

Stolle, C., H. Lühr, M. Rother, and G. Balasis (2006), Magnetic signatures of equatorial spread F as observed by the CHAMP satellite, *J. Geophys. Res.*, 111, A02304, doi:10.1029/2005JA011184.